MECHANICAL AND ELECTRICAL CHARACTERISTICS OF 3D PRINTED MULTI-MATERIAL POLYMER COMPOSITES

Sylvestis Oberoi, Velram Balaji Mohan and Debes Bhattacharyya*

Centre for Advanced Composite Materials, Department of Mechanical Engineering, the University of Auckland, 314 Khyber Pass Road, Private Bag 92019, Auckland, New Zealand

Corresponding author*: d.bhattacharyya@auckland.ac.nz

ABSTRACT

The paper focuses on the investigation of the 3D printing of multi-functional composites using graphene nanoplatelets (GNP) and linear low-density polyethylene (LLDPE). The constituents of the composite used in this study were LLDPE (92wt.%), polypyrrole (PPY) (2wt.%) and graphene nanoplatelets (6wt.%). The investigation adopted a holistic approach to assess the properties of 3D printed GNP-LLDPE composites and compared the composite's mechanical and electrical properties with those of compression moulded composites and neat LLDPE to identify the factors that influence the discrepancies. Hence, a variety of evaluation methods, such as tensile and flexural tests, Fourier Transform Infrared Spectroscopy and dynamic mechanical thermal analysis, have been used to assess the influencing factors. This study showed that the 3D printed composites had excellent mechanical properties, though slightly lower compared to those of compression moulded composites. The nominal increases of 3D printed samples compared to neat polymer were 13.2% (tensile strength), 31.9% (flexural strength), 29.4% (flexural modulus) and 24.7% (storage modulus). Polymethyl methacrylate composites, replacing LLDPE, were also developed by 3D printing, which drastically enhanced mechanical strengths, and electrical and thermal conductivities compared to its compression moulded samples, but those properties were found to be lower compared to those of LLDPE composites.

1. INTRODUCTION

Graphene is a monolayer of sp^2-hybridised carbon atoms firmly bound in a hexagonal honeycomb lattice [1]. It exhibits excellent properties including stiffness, strength, elasticity, high thermal conductivity, extremely high electron mobility and tuneable band gap. Widely known as "wonder material" due to its unprecedented attributes, graphene has gained immense attention among researchers to encourage them further in the fields of graphene derivatives and graphene composites, which has generated a current share of 11% in industry-oriented applications [2]. The presence of graphene as reinforcement can enhance the mechanical/functional and physical/chemical properties for instance conductivity and strength, thus, forming a composite with superior qualities [3]. As compared to its other widely used carbon allotropes, such as graphite and carbon nanotubes (CNTs), the greater specific surface area of graphene allows better interaction with the matrix material whether it is metal, ceramic or polymer [4]. However, relatively low processing temperature and pressure make it easier to fabricate the polymer matrix composites [5]. The past decade has seen a rapid development of 3-dimensional (3D) printing of

SAMPE Conference Proceedings. Charlotte, NC, May 20-23, 2019. Society for the Advancement of Material and Process Engineering – North America.

various polymers, which is a process of creating a 3D object by gradually adding thin layers of thermoplastic polymer in a stack using a 3D computer-aided design model [6].

Numerous studies have reported significant increases in mechanical, electrical, thermal, gas barrier and flame retardant properties of graphene-based polymer composites, as compared to those of the neat polymers [7]. These enhanced properties of the graphene-polymer composites depend on several factors including the type of polymer matrix, concentration and quality of filler as well as dispersity of the filler. These factors are in turn determined by the fabrication techniques employed, for instance, solution mixing, melt-blending and in-situ polymerisation[8]. In addition, during fabrication, uniform mixing of graphene filler and the polymer matrix must be facilitated to achieve the full advantage leading to composites with synergistic properties [9]. The exceptional properties of graphene-polymer composites have opened the doors for their applications in diverse areas, such as energy, electronics, biomedical as well as sensors [10].

As discussed earlier, the dispersity of the filler in the matrix is one of the critical factors influencing the various properties of graphene-polymer composites. Moreover, concerning this subject, numerous studies have reported the challenges to avoid agglomeration of particles in nanocomposites which result in the unwanted disconnection between the nanoparticles. This disconnection eventually induces poor electrical and mechanical properties in the composite. Therefore, to address this issue, hybrid composites come into play [10] which incorporate either a mixture of two or more matrices and a single filler or more in a one matrix or both [11]. Several types of hybrid composites have been developed to cater to a diverse range of applications including sensor devices, solar cells, fuel cells, catalysis and therapeutics [12]. Graphene-based hybrid composites are produced by the cross-linking of graphene or graphene oxide (GO) utilising several types of inorganic or organic species, for instance, inorganic nanoparticles, polymers and multifunctional organic molecules [13].

Due to the relative ease of production in large quantities, most of the graphene-based nanomaterials use GO as a nanoparticle [12]. However, to tailor the properties for required applications, several studies incorporated the use of graphene as a nanoparticle in the hybrid composite. Xu *et al.* [14] produced a hybrid composite consisting of graphene and poly (3,4-ethyldioxythiophene), which showed excellent electrical conductivity beside other superior properties including good flexibility, high thermal stability as well as optical transparency. In addition, Wang *et al.* [15] synthesised graphene-polyaniline hybrid composite using an in-situ polymerisation-reduction processes. Fabricated for supercapacitor application, the composite material not only demonstrated better electrochemical properties but also possessed better energy/power density than the neat constituents.

With the ability to produce complex structures without producing any waste compared to subtractive manufacturing, 3D printing of polymers has found possible applications in aerospace industries for creating complex, lightweight structures, architectural industries for structural models, art fields for artefact replication or education, and medical fields for printing tissues and organs [6]. However, since 3D printed polymer products without any reinforcement lack the strength to be used as fully functional and load-bearing parts, they are often limited to prototype manufacturing [16]. This has led to a proliferation of studies focussing on 3D printed polymer composites to amplify the strength and various other desired properties of the end product. Although, there has been extensive research carried out in the 3D printing of polymer

composites, far too little attention has been paid to 3D printed graphene-polymer hybrid composites except limited empirical investigations concerning properties of 3D printed graphene-polymer hybrid composite products. In addition, the study of 3D printed graphene-linear low-density polyethylene (LLDPE) hybrid composite, and the investigation of their properties have not been reported before. Hence, this study seeks to address these research gaps by explicitly analysing the printability of graphene-LLDPE hybrid composite as well as evaluating the intrinsic mechanical and conductivity properties (electrical and thermal) of its 3D printed samples, based on early research on the development of functional polymer-graphene nanocomposite using LLDPE and polypyrrole (PPY) [17],[18].

1.1 3D Printing

Although 3D printing has been a hot research topic in the past decade or so, most of the research has tended to focus on processing techniques and printing of neat polymers. However, few researchers have been able to carry out research on the 3D printing of polymer-graphene composites. In 2014, a comparative study by Wei *et al.* [19] examined the 3D printing of acrylonitrile butadiene styrene (ABS) and polylactic acid (PLA) composites with different graphene loading (wt.%). They demonstrated for the first time that 3D printing of polymer-graphene composites with graphene loading up to 5.6wt.% was achievable with the composite smoothly extruded from the nozzle. However, discontinuous extrusion was observed for composites with graphene loading of 7.4wt.%. It was claimed that the printer nozzle was clogged at higher graphene loading due to inhomogeneity in the composition. In another study, Zhong *et al.* [20] used graphene oxide and geopolymer nanocomposite for 3D printing. Synthetisation of geopolymer was achieved from a mixture of alkaline source particle and alumina-silicates particles. Their study suggested a successful extrusion of the composite with 10% wt. of graphene oxide loading. Furthermore, in a randomised controlled study, Kim *et al.* [21] printed reduced graphene oxide (rGO) freestanding (without any support) nanowires. GO wires were locally grown at room temperature using the meniscus formed at the tip of a micropipette filled with a colloidal dispersion of GO sheets. GO deposition was obtained by pulling the micropipette as the solvent rapidly evaporated, thus enabling the growth of GO wires. Although the nozzle size of micropipette was 1.3 μm, Kim *et al.* [21] reported a range of diameter sizes in nanometres due to changes in the cross-sections of wires upon stretching of meniscus after being withdrawn from the micropipette. It is apparent that not a single study has reported any work on 3D printing as well as the characteristics of the 3D printed GNP-LLDPE-PPY hybrid composites. Hence, this study seeks to address these research gaps by explicitly analysing the printability of GNP-LLDPE-PPY hybrid composite as well as evaluating the characteristics of 3D printed samples. Further, as evident from the literature [22, 23], although the samples printed with 0° raster angle yield maximum unidirectional properties in the longitudinal direction, they reflect low mechanical properties in the transverse direction. A similar trend is observed in samples printed with 90° raster angle. Therefore, for better isotopic results, this study focuses on 3D printing of GNP-LLDPE-PPY hybrid composite with ±45° raster angle.

2. EXPERIMENTATION

2.1 Materials

The neat polymer, LLDPE of grade Rotathene® 5UV, used in this study was supplied in powder form by Vanglobe, NZ Pty Ltd. In addition, GNP of grade xGnP® M was obtained from Emfutur, Spain. Lansing whereas PPY (product no. 578177) was purchased from Sigma-Aldrich New Zealand Co.

2.2 Fabrication and 3D Printing

Manufacturing of Composites: The GNP-LLDPE-PPY hybrid composites were fabricated using a melt-blending process. The constituents were mixed using a Brabender mixer. For every 50g of constituent mixture, the blending process was carried out for 5 min at 160°C. Specifically, the graphene-LLDPE-PPY hybrid composite utilised in this study consisted of several constituents by percentage weight including LLDPE (92%), PPY (2%) and graphene nanoplatelets (6%).

3D Printable Composite Filament: In order to carry out 3D printing, the material needed to be in the form of a filament with a "uniform" diameter of 1.75mm as per the printer's specifications. Therefore, to begin with, the composite was ground into a powder form and dried in Moreto air drier at 72°C for 12h (as per the machine specifications) to remove any moisture. Since the amount of composite available for this study was relatively small, a conventional extruder was not suitable. Therefore, a Bespoke miniature extruder (purpose-built during the earlier stage [17],[18] was used in conjunction with the conveyor belt, to extrude the composite filament of the uniform desired diameter. The extruder die head was preheated to 230°C, which was controlled with the aid of the thermocouple temperature controller. The air-dried composite granules were then fed into the extruder and left for 4 minutes to ensure the composite's transitions to the glassy state before being extruded. In the extrusion process, although the speed of the conveyor belt was regulated to maintain the uniform tension along the extruded strand, the torque applied manually would introduce the breakages in the strands. Therefore, to counter this problem, a pneumatic pump was used to apply uniform torque, which yielded better results. However, the extruded strands still lacked uniformity in diameter. Therefore, the strands were drawn through a hole of 1.75mm to shave off the excess the material, eventually yielding the desired strands with a uniform diameter of 1.75mm.

3D Printable Polymer Filament: The fabrication process of LLDPE filament started with the drying of LLDPE powder to get rid of any moisture, using the same criteria as were used for the composite. Afterwards, due to the abundant availability of the neat polymer as opposed to that of the composite material, LLDPE extrusion was carried using the Brabender twin screw extruder in conjunction with the conveyor belt to provide required tension for a uniform thickness of the extrudate. Since the polymer is a good thermal insulator, the conveyor belt also featured blowers to ensure the forced cooling of the extrudate, thus preventing it from sticking together during coiling. Before the actual extrusion, the extruder was purged using polypropylene (PP) to get rid of any potential contaminants from its previous use. From the preliminary tests, it was discovered that the unsteady temperature profile along the different zones of the extruder, caused variation in torque applied by the screw due to the material not acquiring the glassy state.

Consequently, this variation in torque pushed the material through the die at fluctuating rates, thus producing the strands of non-uniform diameter. To address this situation, the temperature profile was stabilised by switching the extruder on for 6 hrs prior to the extrusion process. The heating zones of the barrel were maintained in a temperature range of 150°C to 215°C, from the feeding section to the die outlet which ensured the polymer melted gradually. In addition, the pressure inside the barrel was maintained at 27 bar with screw speed set at 140 rpm, which resulted in a relatively stable torque of 73 Nm.

3D Printing: After the production in filament form, the 3D printing of the neat LLDPE and GNP-LLDPE-PPY composite was carried out by using UP Plus-2 3D printer (Tiertime), operated using the proprietary UP Studio software. Upon initial trials of 3D printing with the strands of non-uniform diameter, the results were quite disappointing due to the discontinuous pattern of extrudate coming out of the nozzle. Therefore, after dismantling the printer, it was discovered that the feed mechanism of UP Plus 3D printer consisted of a gear and a bearing. Because of the internal mechanism of the machine only a small variation (± 0.05mm) of the strand diameter could be pushed uniformly, necessitating the need for maintaining a uniform diameter of 1.75mm. The printing was conducted with set parameters including 100% infill, no raft and a layer thickness of 0.25mm. As per the printer specifications, to ensure the best quality of the printed specimens, the printing was carried out at the slowest speed of 10 cm^3/hr. The nozzle of 0.4mm diameter was used, which was to set to 140°C. Furthermore, the platform temperature was set at 100 °C to avoid warping. As evident from the literature review, the 3D printed parts are inevitably anisotropic and contain voids. Therefore, to enhance the interlayer adhesion and reduce anisotropy, the post-processing technique of annealing similar to the one used by Zhang *et al*. [24] was employed. The electric hot air gun was used to blow air at 115°C, which would melt the strips of layers and enhance fusion with the adjacent layers.

Compression Moulded Composites: To fabricate compression moulded GNP-LLDPE-PPY composites, an aluminium mould was fabricated by computer controlled machining for the required dimensions of the composite. The mould cavities incorporated a 2° taper to ensure minimum effort needed during part removal. The compression moulding process was carried out using LabTech 20-tonne heat press. A pre-weighed amount of 250g (enough to fill mould cavity) of polymer composite in the powdered form was placed in the mould cavity. Afterwards, the composite was preheated up to the glass transition temperature of 130°C for 4 min to make the composite softer, thus resulting in the shorter moulding cycle. Furthermore, to allow for gradual compression, the compression stage was divided into two subsequent cycles of 45s and 20s at a pressure of 7MPa. Afterwards, the pressure was released, followed by the cooling cycle of 4 minutes before eventually removing the moulded specimens. To avoid the moulded parts sticking to the mould surface, the mould was cooled down to 50°C for the ease of removal when still slightly hot. Finally, any flash around the moulded parts' edges was removed.

2.3 Characterisations

Tensile Test: To determine the tensile properties, quasi-static tensile tests were carried out using a universal testing machine, Instron 5900 equipped with a 50 N load cell. The tests were conducted according to the ASTM D638-14 [25] standard. Since there was a limited amount of composite material available, the type 5 specimen with a thickness of 2mm was used, as per the standard. Furthermore, with the polymer and composite being semi-rigid, the initial tensile tests

were carried out at a cross-head speed of 100 mm/min For each sample, three specimens were tested at room temperature, and the average tensile strength was obtained directly from the machine using the proprietary Bluehill® Universal software.

Flexural Test: The flexural properties including flexural stiffness and the strength were assessed by conducting a quasi-static three-point flexural test using a universal testing machine, Instron 5900 equipped with a load cell of 50 N. The test was carried out by following Procedure B of ASTM D790-17 [26] standard. Three specimens of each sample with dimensions (40 x 13 x 2 mm), representing a span to thickness ratio of 16:1 (with 20% extra specimen length for an overhang), were tested to account for repeatability and obtain the average values. The support span (30.25mm), as well as the crosshead speed (7.8mm/min), were determined based on the thickness of the specimens following Procedure B. The test was conducted at room temperature of 22.7°C and 52% relative humidity.

Dynamic Mechanical Thermal Analysis: To determine the rheological properties (which are limited to storage modulus) of three different types of specimens including 3D printed composite, compression moulded composite, and 3D printed LLDPE, the DMTA were carried out using TA Instruments Q800. As per the machine's specifications, the test was conducted in a single cantilever mode following ASTM D648-18 [27] standard. According to the standard, the rectangular specimens of dimensions (40 x 13 x 2 mm) were used. With the same conditions used by Fim *et al.* [28], the strain sweep test was performed at a strain of 0.1% strain and frequency of 1 Hz. In addition, the test was conducted in a nitrogen atmosphere within the temperature range of -140°C to 120°C at a heating rate of 3°C/min.

Optical Microscopy: After assessing the mechanical properties, the optical microscopy was used for failure analysis of the failed specimens. The surface structure of the fracture planes was analysed to instigate the microscopic defects, which could potentially validate the empirical results obtained. Hence, the morphology of the 3D printed composite and other two types of specimens used in this study were acquired using a Lecia MZ16 microscope.

Fourier Transform Infrared Spectroscopy (FTIR) analysis was performed on three different samples including 3D printed composite, compression moulded composite, and 3D printed neat LLDPE. The analysis was conducted on Thermo Electron Nicolet iS50 FTIR spectrometer (equipped with smart orbit attenuated total reflectance from Thermo Electron Scientific Instrument Corp., USA. In addition, the data management was performed by the proprietary software, Ominic ESP version 7.1. Conducted in ATR mode, the analysis utilised infrared rays and potassium bromide as a source and beam splitter, respectively. Furthermore, to scrutinise the functional bonds as well as the chemical structure of pyrolysed specimens, each specimen was subjected to 64 consecutive scans at a spectral resolution of 4 cm^{-1}.

Electrical Conductivity values of samples were measured using four-point probe setup. The specimens of dimensions of 90 × 13 × 2mm were used for the tests. Furthermore, the probes were placed at equidistance of 18mm apart.

Thermal Conductivity of the samples was measured using Mathis TC-30Prior to the actual testing, the calibration of the Mathis instrument was carried out using the pre-supplied conventional materials in the calibration kit including high-density polyethylene (HDPE), Pyrex

and Delrin® (Acetal). In addition, to maximise thermal stability, the isothermal chamber was left for 10 min to reach pre-test isothermal equilibrium. The testing was performed in guarded modes using an internal sensor, at a temperature of 30°C. The rectangular specimens with dimensions of 60 x 13 x 2mm were utilised in the experiment with a test duration of 9 min and a cooling period of 5 min. Furthermore, to account for accuracy and precision, the testing involved three replicated tests for each sample.

3. RESULTS

The samples from preliminary 3D printing tests tended to warp around the corners, due to rapid cooling at ambient temperature. It was due to the contraction, creating stresses along the sample's lateral surface. Moreover, the cooling rate of each subsequent layer changes due to the increasing distance from the heated platform. As a consequence, the deformed and lifted corners would displace the part being printed resulting in an adverse outcome. Therefore, to curb this problem, a light draft of hot air at 80°C was created using a hot air gun, around the sample being printed. This lowered the cooling rate of the sample, thus reducing the stresses. In addition, double masking tape was applied on the bed to enhance adhesion of the sample. As discussed before, for each test including flexural, tensile and DMTA, three specimens of the GNP-LLDPE-PPY hybrid composite as well as neat LLDPE were printed in addition to the compression moulded GNP-LLDPE-PPY hybrid composites. Figure 1 illustrates the high quality of the samples yielded from 3D printing. Furthermore, as evident from the optical microscopy images, discussed later, there were relatively few voids present in a row of a single layer. The results are due to the annealing of printed parts performed to enhance interlayer adhesion of printed parts. However, the uniformity of the cross-section with less voids can be further achieved by using a more effective method compared to electric hot air gun, such as an oven for more uniform annealing.

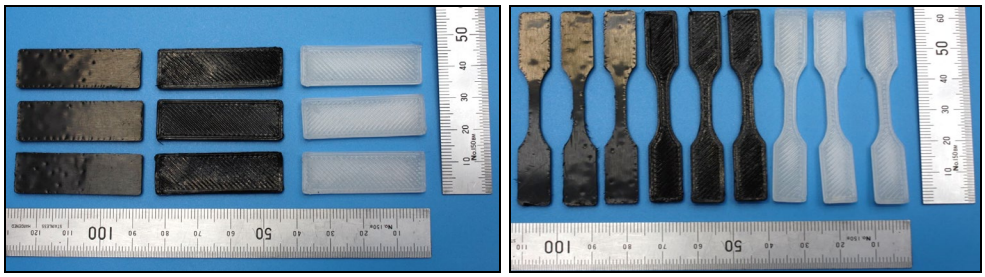

Figure 1: Flexural as well as DMTA test specimens - (a) Compression moulded composite; (b) 3D printed composite; (c) 3D printed LLDPE and Tensile test specimens - (a) Compression moulded composite; (b) 3D printed composite; (c) 3D printed LLDPE

The FTIR spectra of 3D printed LLDPE, compression moulded composite and 3D printed composite are presented in Figure 2. The FTIR spectra of 3D printed LLDPE represent the characteristic peaks at 717cm^{-1} and 1470cm^{-1}, confirming the presence of strong C-Cl halo-compound stretch and N=O nitro-compound stretch respectively [29]. The broad spectra from 1840 cm-1 to 4000 cm-1 represents the functional groups formed by the graphene nanoparticles. Further peaks at 2847cm^{-1} and 2914cm^{-1} in the 3D printed composite spectra suggest the presence of GNP resulting in further bonding due to the presence of additional functional groups. The peaks formed due to added GNP can be attributed to the presence of medium C-H alkanes and aldehyde stretch with an absorbance of 42% and 46%, respectively [29]. Similar results

indicating the further bonding due to the incorporation of GO [30] and graphene sheets [31] in PMMA have been reported. Furthermore, the FTIR data suggest the same spectra for compression moulded composite without any significant changes in the position of the major functionalised groups. However, the peaks at 53% and 56% reflect a slight increase (~10%) in absorbance intensity of the major functionalised groups, indicating a greater number of C-H alkanes and aldehyde stretch bonds in compression moulded composite as compared to a 3D printed composite.

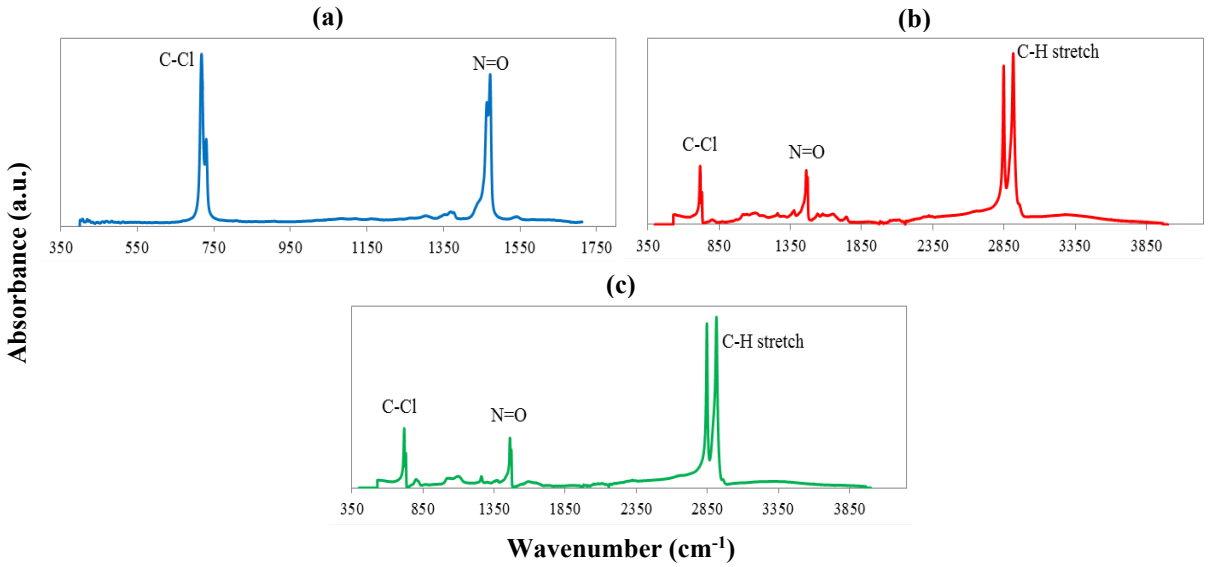

Figure 2: FTIR spectra for 3D printed (a) neat LLDPE, (b) GNP-LLDPE-PPY hybrid composite and (c) compression moulded GNP-LLDPE-PPY hybrid composite

This increase in the number of bonds in compression moulded composite can be the consequence of more tightly packed molecules because of compressive force in the compression moulding process. On the contrary, the 3D printed composite was fabricated by depositing subsequent layers of material, which resulted in unwanted voids, as evident from the morphological results. In addition, there is a slightly higher (2%) infrared absorption (attributed to the oxygen functional group N=O) in compression moulded composite as compared to 3D printed composite. This indicates the presence of slightly bigger defects/voids leading to the agglomeration of oxygen. This is further confirmed by the morphological results. Figure 3 shows the optical microscopic images of the surface structure of the fracture plane of the specimens. The morphological images 3D printed composite indicate the presence of voids aligned in a single layer. On the contrary, printed under the same conditions the morphological images of 3D printed LLDPE specimen do not indicate the presence of any voids. The results may be the consequence of post-processing of printed samples which involved annealing in minimising voids and enhancing better interlayer adhesion as well as reducing anisotropy. However, the individual extrusions and layers are visible in morphological results. This suggests the presence of weak interlayer molecular bonds relative to the tightly packed molecules in compression moulded composite, supported by earlier observations and discussions about FTIR spectra. The uniformity of the cross-section and the reduction of voids can be further improved by using a more effective method compared to electric hot air gun, such as an oven, for more uniform annealing. Furthermore, the morphological images of compression moulded composite indicate

that the presence of voids, possibly resulting due to the trapped air bubbles. The possible explanation for this adverse result is the insufficient pressure for compression moulding. This implies that it might have an adverse impact on the properties of compression moulded composite discussed in the subsequent sections.

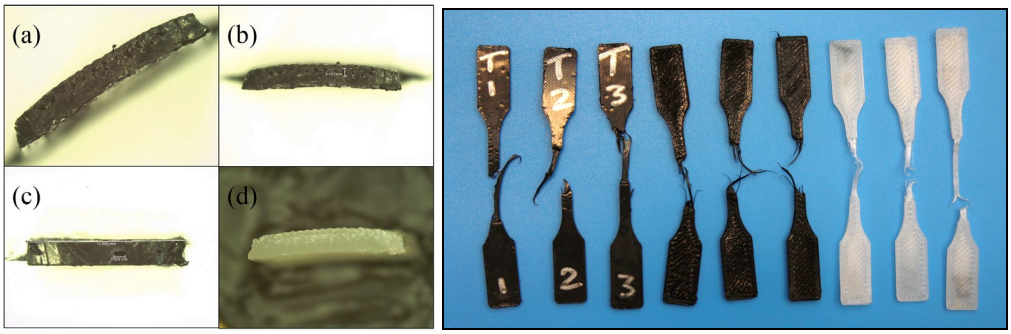

Figure 3: Morphological images of fracture planes of (a) & (b) 3D printed composite; (c) compression moulded composite; (d) 3D printed LLDPE and (e) post tensile test specimens showing the ductile failure after necking

A quasi-static tensile test was carried out using three different sets of specimens to evaluate the tensile properties. As mentioned earlier, due to the limited amount of composite material available, the type 5 specimen was chosen, as per the ASTM D638-14 [25] standard. Therefore, due to the small gauge length (7mm), it was impossible (even using the infrared camera) to capture the accurate data to calculate the tensile modulus. This eventually obscured the analysis and discussion about the effect of graphene filler on the stiffness or elasticity of the 3D printed LLDPE matrix. Hence, only the tensile strength has been reported in this paper. The post tensile test specimens displayed in Figure 4 indicate that all the samples fractured within the gauge length, effectively producing reliable results. Table 1 and Figure 4 show the test results for tensile strength. There is 11.7% increase in tensile strength of printed composite as compared to that of the printed LLDPE, which can solely be attributed to the presence of GNP filler. These results confirm the association with the FTIR results, which indicate the greater intensity of molecular bonds with added graphene. They also corroborate the findings of Shofner *et al.* [32] and Chen *et al.* [33] who reported enhancements in tensile strengths of VGCF-ABS and TPU-PLA matrix composites with added GO loading. On the contrary, a 13.1% reduction in tensile strength of the 3D printed composite is reflected, compared to the compression moulded composite. This discrepancy implies the presence of voids in the microstructure of 3D printed composite, as evident from morphological results, as well as weak interlayer adhesion relative to the compression moulded composite. These voids decrease the effective cross-sectional area, thereby adversely affecting the true strength. Another factor which supports the literature in explaining the difference is the architecture of the printed composite or neat polymer - since the 3D printing was carried out with a raster angle of ±45°, whereas 0° reflects better unidirectional tensile properties [22]. Due to the ductile nature, the specimens did not yield or rupture in the outer surface within 5% strain. Therefore, the three-point flexural test was conducted by the procedure B of ASTM D790-17 [26]. Hence, instead of noting down the results at the yield, the values for maximum flexural strength were obtained at 5% flexure strain.

Table 1: Tensile results for compression moulded composite, 3D printed composite, and 3D printed LLDPE

Specimen #	Width (mm)	Thickness (mm)	Ultimate Tensile Strength (MPa)	
1	3.02	1.99	13.90	Composite (Compression moulded)
2	3.07	1.98	12.20	
3	3.04	1.99	12.70	
Mean	3.04	1.99	12.93	
Standard Deviation	0.03	0.01	0.87	
1		1.96	11.40	Composite (3D printed)
2		2.04	11.10	
3		1.94	11.20	
Mean		1.98	11.23	
Standard Deviation		0.05	0.15	
1	3.31	2.01	10.50	Neat LLDPE (Printed)
2	3.64	2.05	9.86	
3	3.56	2.06	9.79	
Mean	3.50	2.04	10.05	
Standard Deviation	0.17	0.03	0.39	

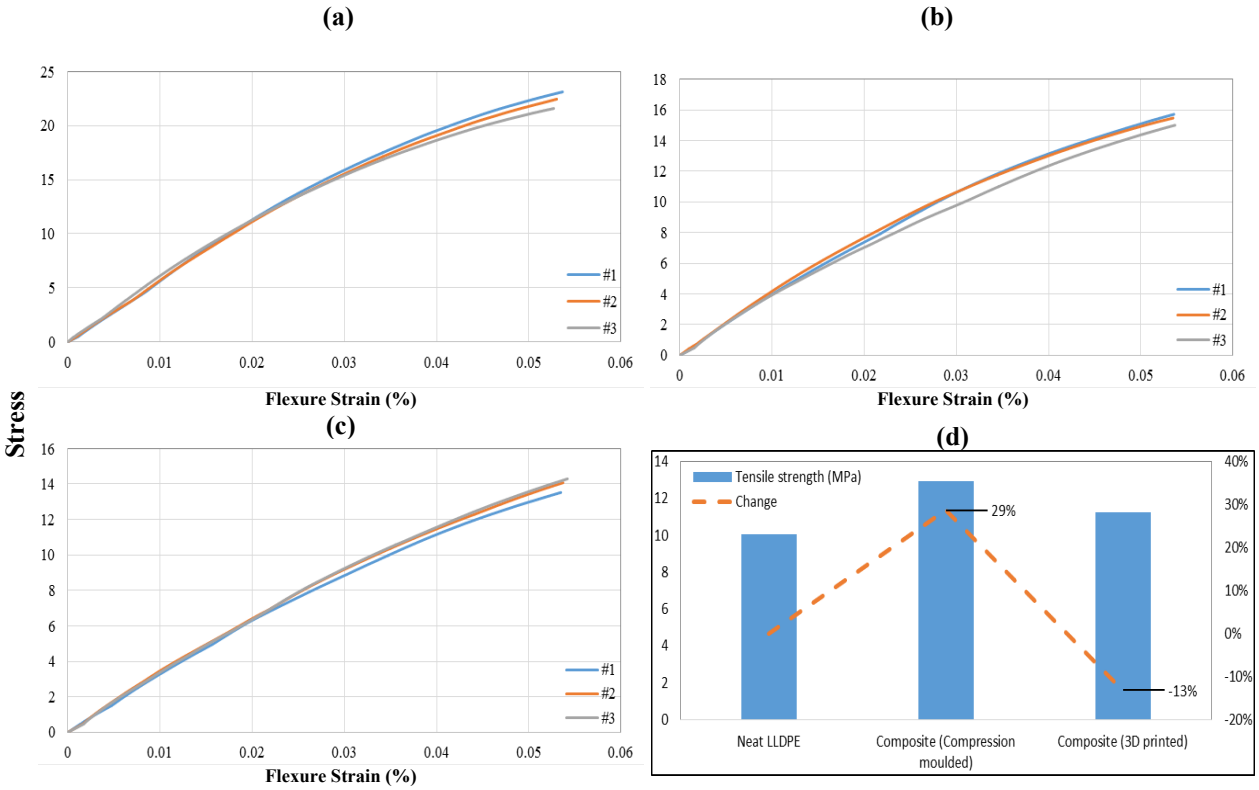

Figure 4: Flexural stress-strain curves for (a) compression moulded composite specimens, (b) 3D printed composite specimens and (c) 3D printed LLDPE specimens and (d) average tensile strength for different types of specimens

Table 2: Flexural results for compression moulded composite, 3D printed composite and 3D printed LLDPE

Specimen #	Width (mm)	Thickness (mm)	Flexural Modulus (MPa)	Flexure stress at 5% Flexure strain (MPa)	
1	12.70	1.95	572.00	22.30	Composite (Compression moulded)
2	12.66	1.96	560.00	21.80	
3	12.65	1.98	611.00	21.10	
Mean	12.67	1.96	581.00	21.73	
Standard Deviation	0.03	0.02	26.66	0.60	
1	12.56	2.00	404.00	15.10	Composite (3D Printed)
2	12.57	1.97	423.00	14.90	
3	12.89	1.95	403.00	14.40	
Mean	12.67	1.97	410.00	14.80	
Standard Deviation	0.19	0.03	11.27	0.36	
1	12.73	1.97	329.00	13.00	Neat LLDPE (3D Printed)
2	12.71	1.97	351.00	13.40	
3	12.74	2.00	342.00	13.60	
Mean	12.73	1.98	340.67	13.33	
Standard Deviation	0.02	0.02	11.06	0.31	

The results indicate about 11% and 20.4% (Figure 5) increases in the flexural strength and modulus, respectively, for printed composite as compared to those of printed LLDPE. The increase in the flexural modulus, as evident from the increased slope of stress-strain curves, indicate that the printed composite is stiffer or more resistant to deformation under flexure load. A possible explanation of this increase in modulus is the presence of GNP filler, which is further confirmed from FTIR results. On the flipside, a 31. 9% and 29.4% (Table 2) reductions in flexural strength and modulus. Respectively, of the 3D printed composite take place. Several factors can explain this observation. Firstly, there are fewer voids and more tightly packed molecules in compression moulded specimens, as evident from the morphological images. Secondly, the higher intensities of peaks observed in FTIR spectra of compression moulded composite relative to those of 3D printed composite, further strengthen the reasoning behind the increased number of bonds.

Figure 6a shows the storage modulus of different specimens including compression moulded composite, 3D printed composite and neat LLDPE. It is apparent from the DMA curves, there is a rapid drop in storage modulus of all three types of specimens from -140°C to -90°C. This implies that the samples softened rapidly and consequently lost the stiffness due to breakage of crosslinking chains and bonds. However, there is a relatively gradual decrease in stiffness once the temperature increases up to 120°C. In addition, there is an increase in storage modulus of both the compression moulded composite and printed composite as compared to printed neat LLDPE. The 20.7% increase in storage modulus of printed composite as compared to that of printed neat LLDPE can be attributed to the presence of GNP.

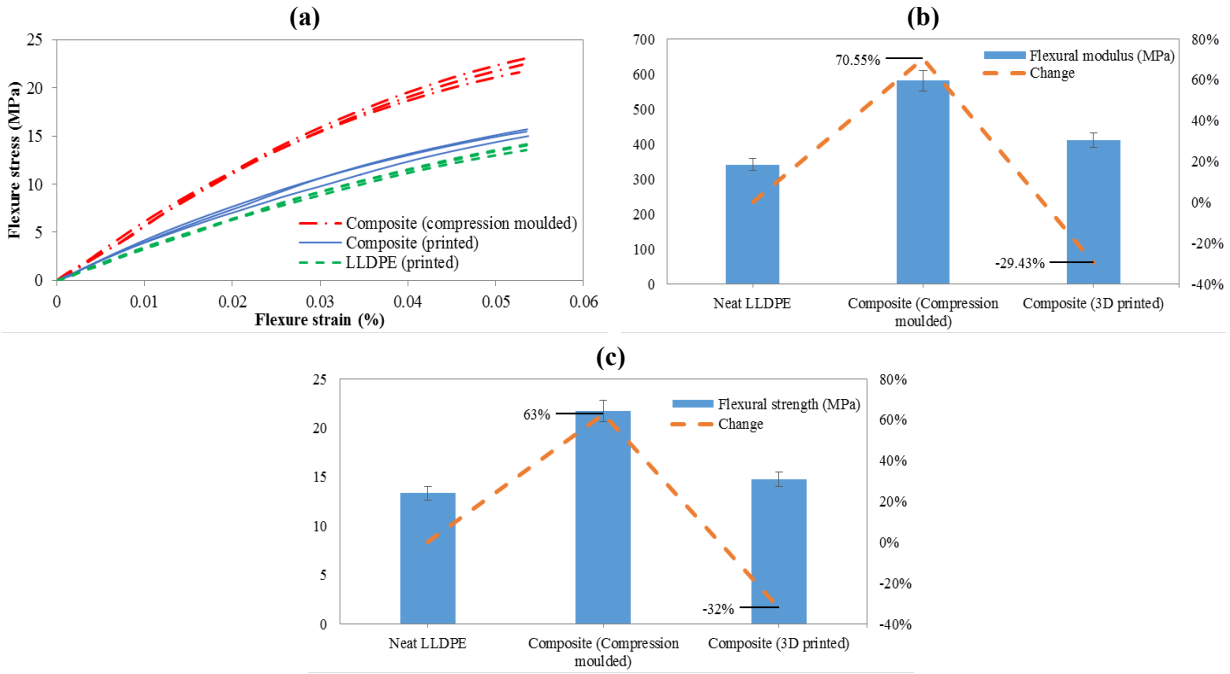

Figure 5: (a) Flexural stress-strain curves for 3D printed composite, 3D printed LLDPE and compression moulded composite specimens, (b) average flexural modulus for different types of specimens and (c) average flexural strength for different types of specimens

In addition, these results are in agreement with those obtained by Wei *et al.* [19] and Chen *et al.* [34] who reported increases in storage moduli of printed ABS composite with rGO and GNP filler, respectively. A further 24.7% increase in storage modulus of compression moulded composite is observed as compared to that of printed composite. This can be attributed to a higher degree of crosslinking as well as covalent bonds formed by GNP, which was confirmed by FTIR spectra. Additionally, these results confirm the association with the previous findings of flexural modulus which show a similar trend regarding the effects of GNP filler.

As apparent from Figure 6b, since LLDPE is an electrical insulator [35], it implies that the inherited conductivity in both the compression moulded composite and 3D printed composite is due to the presence of GNP. These results are consistent with the results reported by Leigh *et al.* [36] and Wei *et al.* [19]. In addition, the electrical conductivity of the 3D printed composite is 7.9% higher than that of compression moulded composite. One possible explanation for this interesting result is the better alignment of sp2 hybridised carbon atoms of graphene in 3D printed specimen, thus increasing the capacity to transfer the electric charge. Further, as discussed previously, there is a slightly higher infrared absorption attributed to the oxygen functional group N=O in compression moulded composite as compared to 3D printed composite. This indicates structural defects/voids leading to agglomeration of oxygen, which is an electrical insulator. In addition, since the transport of electric charge depends on the electron mean free path, any defects act as scattering sites for the electrons, thus reducing the electrical conductivity [37].

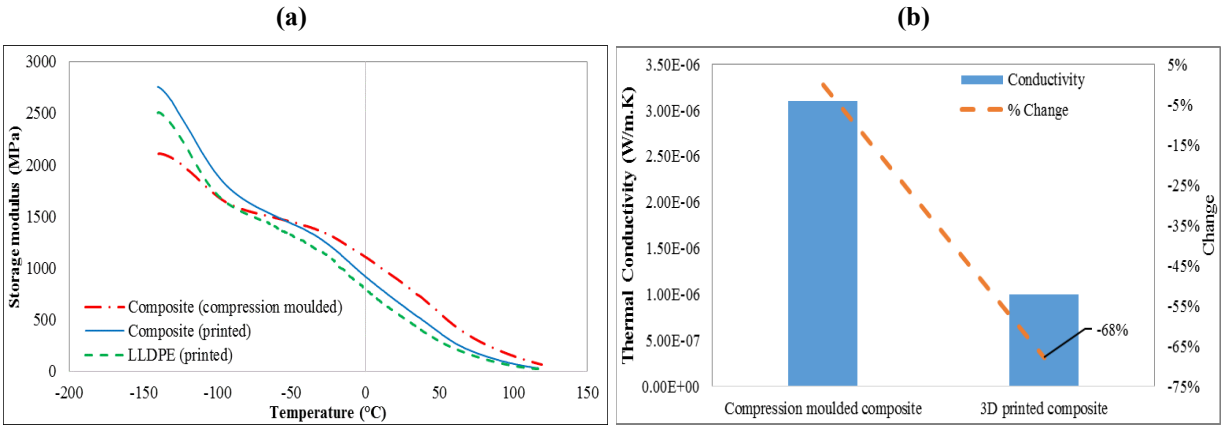

Figure 7: (a) Storage modulus of different specimens and (b) average electrical conductivity and thermal conductivity for compression moulded and 3D printed composite

LLDPE is a heat insulator, with a negligible thermal conductivity due to its amorphous state [38]. Therefore, it is inferred that the increase in thermal conductivity of both the composites (compression moulded and 3D printed) is solely due to the presence of GNP. This substantiates previous findings in the literature which reported an increase in thermal conductivity of graphene-based polymer composites [7]. The thermal conductivity of the 3D printed composite is 0.000001 W/m.K whereas the compression moulded composite had a thermal conductivity of 0.0000031 W/m.K which is rather interesting as showed in Table 3. A possible explanation based on the literature is the presence of voids in 3D printed composite (as evident from the morphological results) which introduces phonon scattering [39].

Table 4: Summary of results

Property	Composite (Md)	Composite (Pr)	LLDPE (Pr)	Composite (Md → Pr)	Pr LLDPE → Pr Composite
Tensile strength (MPa)	12.93	11.23	10.05	▼ -13.15%	▲ 11.74%
Flexural strength (MPa)	21.73	14.8	13.33	▼ -31.89%	▲ 11.03%
Flexural modulus (MPa)	581	410	340.67	▼ -29.43%	▲ 20.35%
Storage modulus (MPa)	880.24	663.24	549.37	▼ -24.65%	▲ 20.73%
Electrical conductivity (S/cm)	0.000278	0.0003	-	▲ 07.91%	-
Thermal conductivity (W/m.K)	0.0000031	0.000001	-	▼ -67.74%	-
*Composite (Md) – Compression moulded composite; Composite (Pr) – 3D printed composite; LLDPE (Pr) – 3D printed LLDPE					

4. CONCLUSIONS

This study has presented the mechanical properties, as well as the electrical and thermal conductivity values of 3D printed GNP-LLDPE-PPY hybrid composite with a 6 wt.% graphene loading and 2 wt% PPY. The methodology involved adopting a holistic approach did produce good quality material to be successfully 3D printed. The properties of 3D printed GNP-LLDPE-PPY hybrid composites have been compared with those of compression moulded GNP-LLDPE-PPY hybrid composite and 3D printed neat LLDPE. The results of the investigation have shown

that the addition of GNP can enhance the mechanical properties of the 3D printed composites as compared to 3D printed neat LLDPE with an increase of 11.7% in tensile strength, 11% in flexural strength, 20.4% in flexural modulus and 20.7% in storage modulus. As expected, this study has shown lower mechanical properties of 3D printed composites relative to those of compression moulded composites. There have been reductions of 13.2% in tensile strength, 31. 9% in flexural strength, 29.4% in flexural modulus and 24.7% in storage modulus. A similar trend has also been observed in thermal conductivity with a significant reduction of 68% due to voids in the 3D printed samples. On the contrary, the research has shown a 7.9% increase in electrical conductivity of 3D printed composite as compared to that of compression moulded composite. The findings of this investigation complement those of earlier studies in the field of graphene-based polymer hybrid composites. The principal theoretical implication of this study is that although GNP filler enhanced the mechanical properties as well as conductivity values (electrical and thermal) of printed composites compared to 3D printed LLDPE, they still exhibit lower values in comparison to those of the compression moulded composite. The study provides a first comprehensive assessment of its mechanical properties and conductivity (electrical and thermal) of the 3D printed products using stated materials. The scope of this study was limited in terms of 3D printing of specimens with a ±45° raster angle. Hence, further studies need to be carried out to investigate the degree to which the properties of the 3D printed GNP-LLDPE-PPY hybrid composite will vary with 0° and 90° raster angle.

ACKNOWLEDGEMENT
The authors would like to thank the Ministry of Business, Innovation and Employment (UOAX1415), New Zealand for the financial support.

5. REFERENCES

[1] V. B. Mohan, K.-t. Lau, D. Hui, D. Bhattacharyya, Composites Part B: Engineering 2018.
[2] B. L. Dasari, J. M. Nouri, D. Brabazon, S. Naher, Vol. 140, 2017, 766.
[3] A. Nieto, A. Bisht, D. Lahiri, C. Zhang, A. Agarwal, International Materials Reviews 2017, 62, 241.
[4] X. Zhao, Q. Zhang, D. Chen, P. Lu, Macromolecules 2010, 43, 2357.
[5] S. R. Bakshi, D. Lahiri, A. Agarwal, International Materials Reviews 2010, 55, 41.
[6] X. Wang, M. Jiang, Z. Zhou, J. Gou, D. Hui, Composites Part B: Engineering 2017, 110, 442.
[7] T. K. Das, S. Prusty, Polymer-Plastics Technology and Engineering 2013, 52, 319.
[8] V. B. Mohan, R. Brown, K. Jayaraman, D. Bhattacharyya, Advanced Composite Materials 2018, 27, 349.
[9] V. B. Mohan, K. T. Lau, D. Hui, D. Bhattacharyya, Composites Part B: Engineering 2018, 142, 200.
[10] V. B. Mohan, K. Jayaraman, D. Bhattacharyya, International Journal of Smart and Nano Materials 2016, 7, 179.
[11] K. L. Mittal, *Progress in adhesion and adhesives*, John Wiley & Sons, 2015.
[12] J. Park, H. S. N. Jayawardena, X. Chen, K. W. Jayawardana, M. Sundhoro, E. Ada, M. Yan, Chemical Communications 2015, 51, 2882.
[13] D. Zhou, Y. Cui, B. Han, Chinese science bulletin 2012, 57, 2983.
[14] Y. Xu, Y. Wang, J. Liang, Y. Huang, Y. Ma, X. Wan, Y. Chen, Nano Research 2009, 2, 343.
[15] H. Wang, Q. Hao, X. Yang, L. Lu, X. Wang, Nanoscale 2010, 2, 2164.
[16] C. Soldano, A. Mahmood, E. Dujardin, Carbon 2010, 48, 2127.
[17] V. Mohan, Development of Functional Polymer-Graphene Nanocomposites 2016.

[18] X. Huang, Z. Yin, S. Wu, X. Qi, Q. He, Q. Zhang, Q. Yan, F. Boey, H. Zhang, small 2011, 7, 1876.
[19] X. Wei, D. Li, W. Jiang, Z. Gu, X. Wang, Z. Zhang, Z. Sun, Scientific reports 2015, 5, 11181.
[20] J. Zhong, G.-X. Zhou, P.-G. He, Z.-H. Yang, D.-C. Jia, Carbon 2017, 117, 421.
[21] J. H. Kim, W. S. Chang, D. Kim, J. R. Yang, J. T. Han, G. W. Lee, J. T. Kim, S. K. Seol, Advanced Materials 2015, 27, 157.
[22] T. Letcher, M. Waytashek, "Material property testing of 3D-printed specimen in PLA on an entry-level 3D printer", presented at *ASME 2014 international mechanical engineering congress and exposition*, 2014; Y. Song, Y. Li, W. Song, K. Yee, K.-Y. Lee, V. Tagarielli, Materials & Design 2017, 123, 154.
[23] S. A. Tronvoll, T. Welo, C. W. Elverum, The International Journal of Advanced Manufacturing Technology 2018, 1.
[24] M. Zhang, X. Song, W. Grove, E. Hull, Z. Pei, F. Ning, W. Cong, "Carbon nanotube reinforced fused deposition modeling using microwave irradiation", presented at *ASME 2016 11th International Manufacturing Science and Engineering Conference*, 2016.
[25] A. Standard, Standard test method for tensile properties of plastics. ASTM International, West Conshohocken, PA.
[26] A. Standard, Standard Test Methods for Flexural Properties of Unreinforced and Reinforced Plastics and Electrical Insulating Materials[1]. ASTM International, West Conshohocken, PA.
[27] A. Standard, Standard Test Method for Deflection Temperature of Plastics Under Flexural Load in the Edgewise Position. ASTM International, West Conshohocken, PA.
[28] F. d. C. Fim, N. R. Basso, A. P. Graebin, D. S. Azambuja, G. B. Galland, Journal of Applied Polymer Science 2013, 128, 2630.
[29] M. A. Mohamed, J. Jaafar, A. Ismail, M. Othman, M. Rahman, in *Membrane Characterization*, Elsevier, 2017, 3.
[30] S. N. Tripathi, P. Saini, D. Gupta, V. Choudhary, Journal of Materials Science 2013, 48, 6223.
[31] S. Mohamadi, N. Sharifi-Sanjani, H. Mahdavi, Journal of Macromolecular Science, Part A 2011, 48, 577.
[32] M. Shofner, K. Lozano, F. Rodríguez-Macías, E. Barrera, Journal of applied polymer science 2003, 89, 3081.
[33] Q. Chen, J. D. Mangadlao, J. Wallat, A. De Leon, J. K. Pokorski, R. C. Advincula, ACS applied materials & interfaces 2017, 9, 4015.
[34] S. Dul, L. Fambri, A. Pegoretti, Composites Part A: Applied Science and Manufacturing 2016, 85, 181.
[35] P. N. Khanam, M. AlMaadeed, M. Ouederni, E. Harkin-Jones, B. Mayoral, A. Hamilton, D. Sun, Vacuum 2016, 130, 63.
[36] S. J. Leigh, R. J. Bradley, C. P. Purssell, D. R. Billson, D. A. Hutchins, PloS one 2012, 7, e49365.
[37] M. Acik, G. Lee, C. Mattevi, M. Chhowalla, K. Cho, Y. Chabal, Nature materials 2010, 9, 840.
[38] X. Huang, P. Jiang, T. Tanaka, IEEE Electrical Insulation Magazine 2011, 27.
[39] A. Li, C. Zhang, Y.-F. Zhang, Polymers 2017, 9, 437.